Characterization of Fuel and Cladding In and Near the Pellet–pellet Gap of a High-Burnup Pressurized Water Reactor Fuel Rod

ROSE MONTGOMERY,[1] JASON HARP, BRUCE BEVARD, TYSON JORDAN
Oak Ridge National Laboratory, One Bethel Valley Road, Oak Ridge, TN 37831
[1]montgomeryra@ornl.gov

GUIRONG PAN, DAVID B. MITCHELL
Westinghouse Electric Company, Columbia, SC 29223

TOM BROOKMIRE, CHRISTOPHER CLEMENS
Dominion Energy Services Inc., Richmond, VA 23060

MUHAMMET AYANOGLU
ORANO TN LLC, Columbia, MD 21046

At TopFuel 2021, we reported on metallographic examinations of a high-burnup ZIRLO-clad spent fuel rod operated at the North Anna Power Station having a 3 mm gap between pellets at an elevation of ~1403 mm. The rod was sectioned axially at that elevation to reveal the pellet–pellet interfaces and the pellet–pellet gap. Sections were mounted and polished to reveal the distribution of cladding inner and outer oxide layer thicknesses above, below, and within the gap. Since then, total cladding hydrogen measurements have been performed to quantify the cladding hydrogen content through the gap and above and below the pellet–pellet gap region. This paper provides the cladding hydrogen concentrations and discusses the overall findings regarding cladding waterside oxidation and cladding hydrogen diffusion to a pellet–pellet gap. The results of the study indicate that hydrogen diffused to the pellet–pellet gap, but only from the elevation just below the gap. The magnitude of the diffusion was not enough to increase the gap cladding hydrogen content to the concentration of the cladding above and below it, and the hydrogen concentration remained lower than typical for that rod elevation.

1 Introduction

During earlier nondestructive examinations, a ZIRLO-clad fuel rod (3D8E14) was identified by gamma scan as having a pellet–pellet gap in the pellet stack at ~1403 mm rod elevation. The estimated burnup of this rod elevation is 64 GWd/MTU, and the rod is from a batch fuel assembly used for typical reactor operation at the North Anna Power Station.

To characterize the rod in and near the pellet–pellet gap, the as-discharged fuel rod was segmented around the gap location, as illustrated in Figure 1. The specimen was then cut longitudinally to reveal the pellets and the gap, and microscopy was completed above, below, and in the gap area [1]. The removed cladding section was reserved for total hydrogen measurements. The image of the pellets above and below the gap, and the gap itself, are shown in Figure 2. Higher magnification images showing the cladding hydride distributions are provided in Figure 3.

Montgomery et al. [1] describe the microscopy completed and discuss the observed circumferential cladding hydride distributions, which included a rim near the cladding outer diameter (OD) and inner diameter (ID). Visually, the hydride density in the gap region did not appear to be increased beyond what was observed in areas away from the pellet–pellet gap. The initial inspections further established (1) the expected pellet axial and radial crack patterns, (2) high-burnup rims at the pellet OD and chamfers, (3) pellet bonded regions where pellet–cladding interaction occurred (4) creep of the cladding into the pellet–pellet gap region, and (5) a thinner OD oxide layer within the gap region. Although some rods were heat-treated

for dry storage vacuum drying conditions in the hot cell, this rod was not heat-treated. Therefore, the only opportunity for temperatures high enough to support diffusion would have occurred during reactor operation.

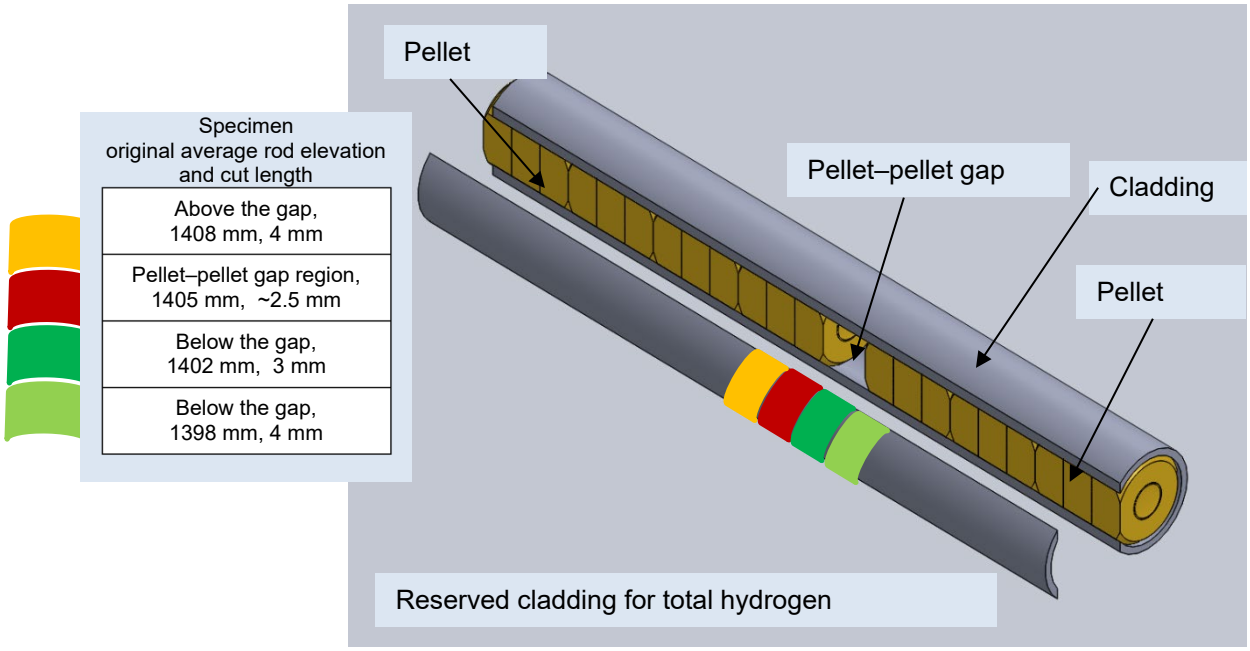

Figure 1. Segmentation of the parent rod around the pellet–pellet gap with the longitudinal subsection reserved for cladding hydrogen measurements and its subsections for LECO analysis.

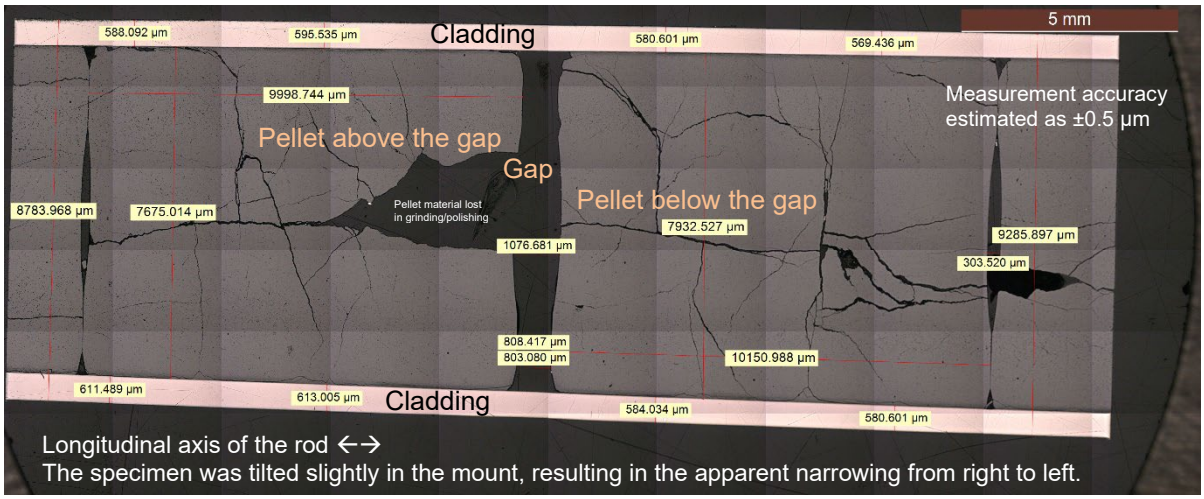

Figure 2. A pellet–pellet gap at ~1,403 mm elevation in fuel rod 3D8E14 (circa 1996).

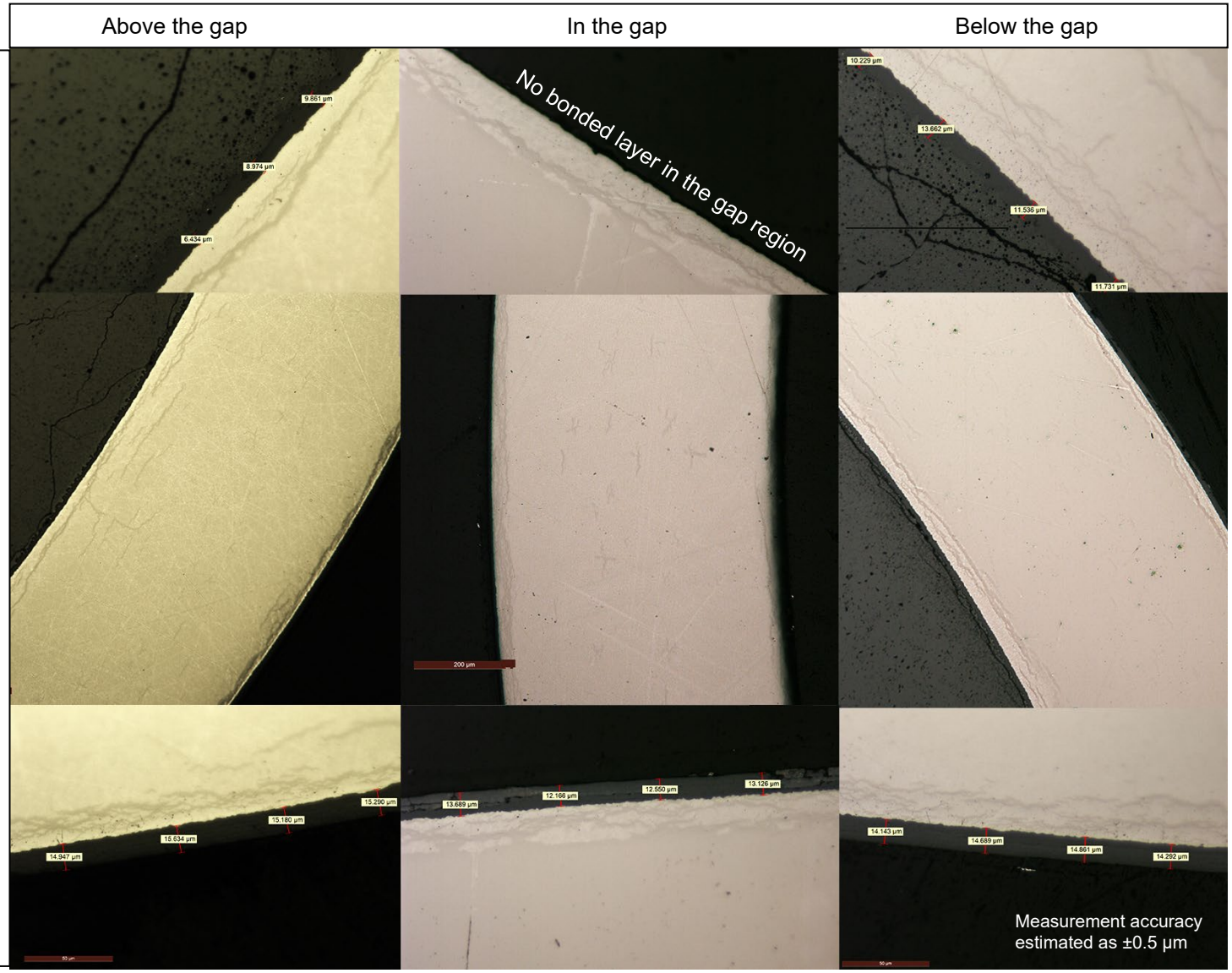

Figure 3. Magnified views of the cladding and pellet cross-section below, in, and above the pellet–pellet gap.

2 Background

It has long been recognized that hydrogen is picked up by cladding through the oxidation process, and, at temperatures above the solubility limit, hydrogen in solution can diffuse to different locations via concentration, temperature, and stress gradients. Much research has been focused on the diffusion of hydrogen in zirconium-based alloys used in reactor cladding, and simulation codes have been developed to predict the migration of hydrogen associated with reactor operations. For example, Courty, Motta, and Hales [2] presented a BISON hydrogen model that incorporated the influence of cladding hydrogen concentration and temperature gradients, as well as observed hysteresis in the dissolution/precipitation of zirconium hydrides, to predict the movement of hydrogen associated with power operations. More recently, projects such as the SPIZWURZ project [3] are investigating hydrogen diffusion in gradients associated with dry storage of spent fuel.

The accurate predictive capability for hydrogen dissolution, diffusion, and precipitation is important to establish fuel cladding performance during its operating lifetime and in storage and disposal environments. However, most prior works are based on continuum gradients using empty cladding or flat coupons. The present observations offer the potential for corroborating or contradictory evidence based on the whole fuel system. During operation, there is a typical temperature and concentration gradient at every pellet–pellet interface. Additionally, the fuel pellets are hour-glassed, which creates local stress and strain gradients. Hydrogen trapping in the stress gradients at the pellet ends is a possible deterrent to hydrogen diffusion into pellet–pellet interfaces and gaps.

3 Hydrogen concentration measurement and uncertainty

A LECO Model 836ONH was used for the total cladding oxygen and hydrogen measurements. The LECO analyzer uses a destructive method, the inert gas fusion technique, to analyze elemental oxygen, nitrogen, and hydrogen content. The specimen is melted, thus liberating the oxygen, nitrogen, and hydrogen, which are captured in a helium carrier gas and moved through the LECO system for quantification. The measurements include hydrogen in the cladding alloy and in the waterside and pelletside oxide layers, as well as the oxygen in the waterside and pelletside oxide layers.

The cladding samples for hydrogen analysis were subsectioned from the gap specimen as indicated in Figure 1. For other rods, and for samples from other elevations of this rod, each specimen was subsectioned into four quadrants around the circumference of the cladding at 0°, 90°, 180°, and 270°. Although the quadrants cannot be traced to the position in the reactor, the azimuthal measurements can indicate some variations in cladding hydrogen content resulting from in-reactor temperature differences around the rod's circumference.

The sample mass from the gap cladding section was necessarily slightly under the target 0.1 g established for ORNL cladding measurements but was well within the calibrated response of the system. Figure 4 shows the range of specimen mass used in the test campaign, and no trends or biases were evident within the sample measured hydrogen concentration.

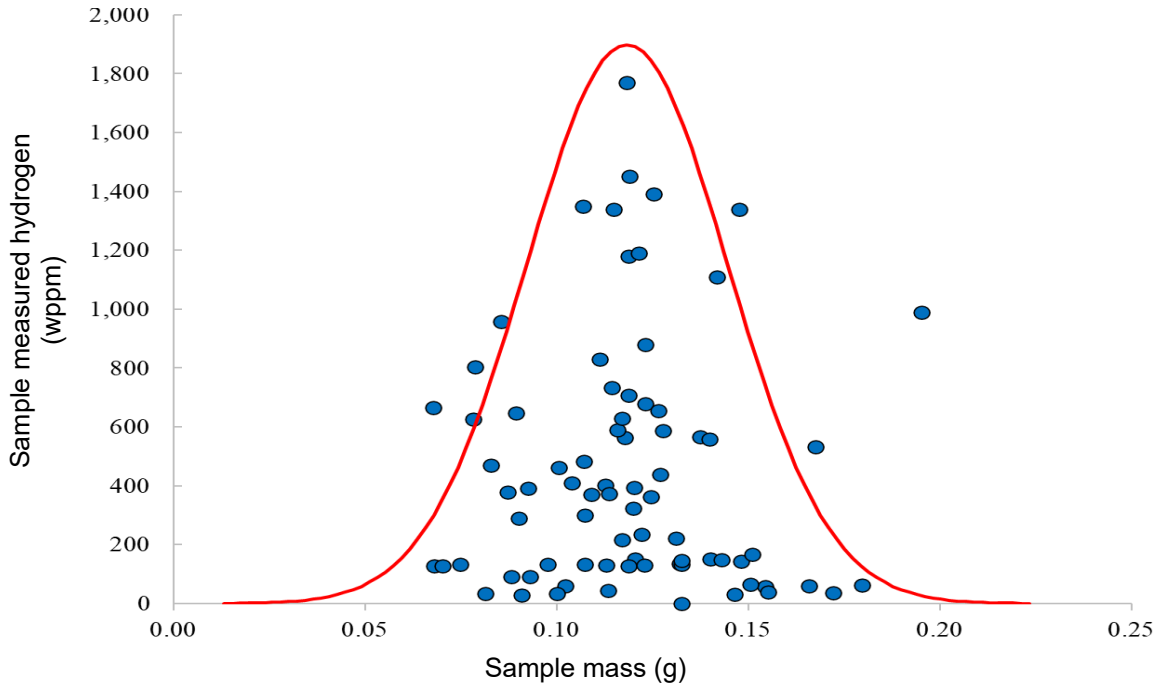

Figure 4. Measured hydrogen as a function of specimen mass: no trends were observed.

The standard LECO refractory metals test procedure was modified slightly to reduce the carbon contamination generated by each test. In this modified method, a LECO 782-720 high-temperature crucible is filled with approximately 0.050 g of graphite powder. The graphite powder is used to ensure good thermal contact between the nickel capsule and the graphite crucible when the capsule drops into the furnace. The instrument is fitted with a LECO 782-721 lower electrode tip that supplies the current to melt the specimen. Samples are placed in a LECO 502-344 nickel basket or a LECO 502-822 nickel capsule for analysis, and the remaining metallic slag is disposed of after the test. Before each batch of cladding specimens is tested, the system is calibrated using four Ti and Zr standards that have certified hydrogen content ranging from 9 to 290 wppm. To calibrate for hydrogen content higher than 290 wppm, multiple calibration standards are used for a single calibration measurement up to the system's ability to completely melt the specimens (more than four calibration standards). These standards or combination of standards are selected to bound the system response of the measured samples.

Typically, industrial users of the LECO machine cite a measurement uncertainty based on the standard deviation of multiple samples from the same specimen, but multiple samples cannot be tested for irradiated cladding samples, and an assessment of the uncertainty of each sample measurement is problematic. For example, although the quadrant samples measured at some elevations could be broadly grouped as duplicate samples with a standard deviation calculated from the four, waterside cladding oxidation and the resulting associated hydrogen content can vary azimuthally. Consequently, estimating uncertainty based on the quadrant variation is overly conservative. Alternatively, the estimated uncertainty can be based on the deviation of the calibration standard measurements from their certified content; however, the maximum relative error associated with the calibration standard measurements is ±0.5%, which is unrealistically low. Therefore, neither approach is considered particularly accurate.

Rather than assessing uncertainties that are not accurate for each measurement, the group of cladding measurements from several similar rods, with several elevations per rod and four quadrants per elevation, are provided for comparison. The data are fit using the least squares method, and the residuals are used to generate a standard deviation.

4 Measurement results

The specimen harvested from the rod in the pellet–pellet gap region, as shown in Figure 1, was subsectioned into four samples—one above the gap, one in the gap, and two below the gap—to cover the range of rod elevations from 1396 to 1409 mm. The oxygen and hydrogen results are provided in Table I. Samples were also taken from two other elevations of rod 3D8E14 at 2665 and 3216 mm, and the results are listed in Table I for comparison. The measured data are plotted hydrogen concentration versus the oxygen concentration in Figure 5, and the hydrogen concentration is plotted as a function of rod elevation in Figure 6.

Additionally, a similar rod (3F9N05) having the same cladding alloy and operated in the same reactors was analyzed using the same LECO machine. Rod 3F9N05 was almost identical in design to rod 3D8E14 but was operated in different cycles; rod 3F9N05's first cycle was the same cycle as rod 3D8E14's third and final cycle of operation. The similarities in fabrication and operation make 3F9N05 a good comparator for rod 3D8E14, and the data are shown in Figure 5 and Figure 6 as an additional point of comparison. Furthermore, Pacific Northwest National Laboratory (PNNL) also measured hydrogen content in ZIRLO cladding for similar rods operated in the same reactors, and the measurements from these samples are included in the plots [4,5]. These data were all used to generate the standard deviations shown in the graphs.

The hydrogen concentration of all four of the cladding samples in and near the gap qualitatively have the expected hydrogen concentration (around 200 wppm or less), which is four times lower than 3D8E14's peak rod hydrogen concentration (on the order of 800 wppm). The oxide thickness at the gap region (~14 μm) is within the typical range for ZIRLO-clad rods at this rod elevation.

5 Discussion

Referring to Figure 6, the oxide thickness, and therefore the cladding hydrogen concentration, follows a general trend with rod elevation. The true correlating parameter is the cladding temperature during reactor operation, not the rod elevation. However, because the coolant temperature increases almost linearly from the bottom to the top of the reactor core and these rods were operated near the same power levels, the rod elevation can be used for general trending.

The LECO measures oxygen and hydrogen content independently. The waterside oxide layer is the primary source of the oxygen measured, and this is further verified by the data. As shown in Figure 7, the measured waterside oxide layer thickness is highly correlated to the measured oxygen concentration. Because the hydrogen in the cladding evolves via the in-reactor oxidation process, and the measured oxygen corresponds to the oxide layer on the cladding, the oxygen and hydrogen contents are also closely correlated, as shown in Figure 5.

If no diffusion occurred, then the gap region is expected to have lower oxygen and lower hydrogen than other elevations of the cladding because the gap region would have had a lower temperature during operation yielding less local oxidation and less cladding hydrogen pickup. In this case, the measured oxide layer is only about 3 μm thinner (see Figure 3), but the lower oxidation thickness is still visible as a darker band on the waterside surface of the rod, as shown in Figure 8. If diffusion did occur, then the gap region should have lower oxygen (because there was less local waterside oxidation in the area), but there should be a hydrogen concentration consistent with the nearby above-gap or below-gap regions.

At the 1405 mm rod elevation and without a pellet–pellet gap, given the trends established in Figure 5 to Figure 7, the waterside oxide thickness is typically 16 μm, the expected oxygen concentration is about 10,600 wppm, and the hydrogen concentration is 144 wppm (by rod elevation) to 180 wppm (by oxygen concentration/oxide thickness).

Table I. Measured cladding oxygen and hydrogen content (wppm)

Segment ID	Specimen average elevation (mm)	Specimen mass (g)	Local measured average oxide thickness (μm)	Oxygen content (wppm)	Hydrogen content (wppm)
3D8E14-1375-1450, pellet–pellet gap elevation	1398	0.1126	14.9	11,000	157
	1402	0.0752		15,600	216
	1405 (gap)	0.1101	12.0	4,850	115
	1408	0.1227	12.9	9,750	131
3D8E14-2655-2674	2665 0° quadrant	0.1245	34.4	14,600	363
	2665 90° quadrant	0.1200		14,500	323
	2665 180° quadrant	0.1276		16,600	587
	2665 270° quadrant	0.1186		17,600	708
3D8E14-3206-3225	3216 0° quadrant	0.1230	49.0	21,900	678
	3216 90° quadrant	0.1264		20,700	654
	3216 180° quadrant	0.1375		20,400	567
	3216 270° quadrant	0.1177		20,300	564

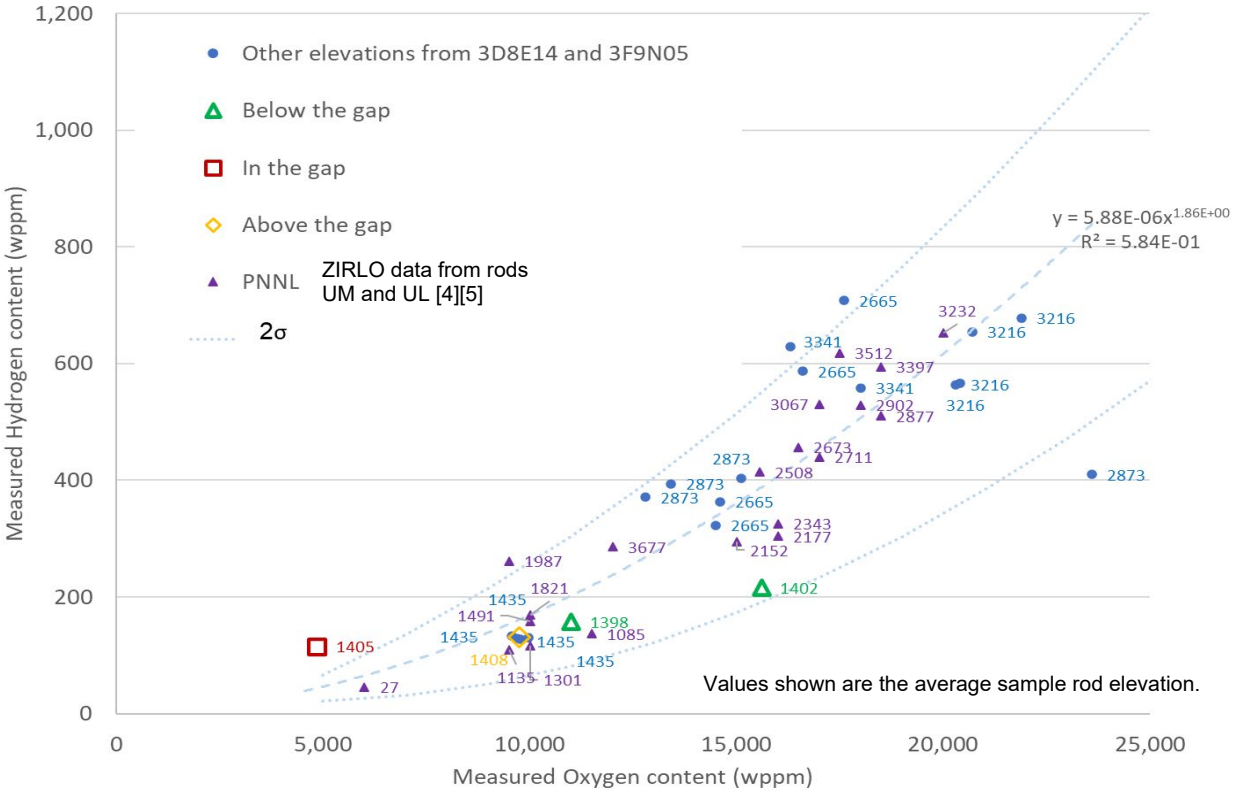

Figure 5. Measured oxygen vs. hydrogen content for above, below, and in the pellet–pellet gap compared with data from the same and other comparable ZIRLO-clad rods.

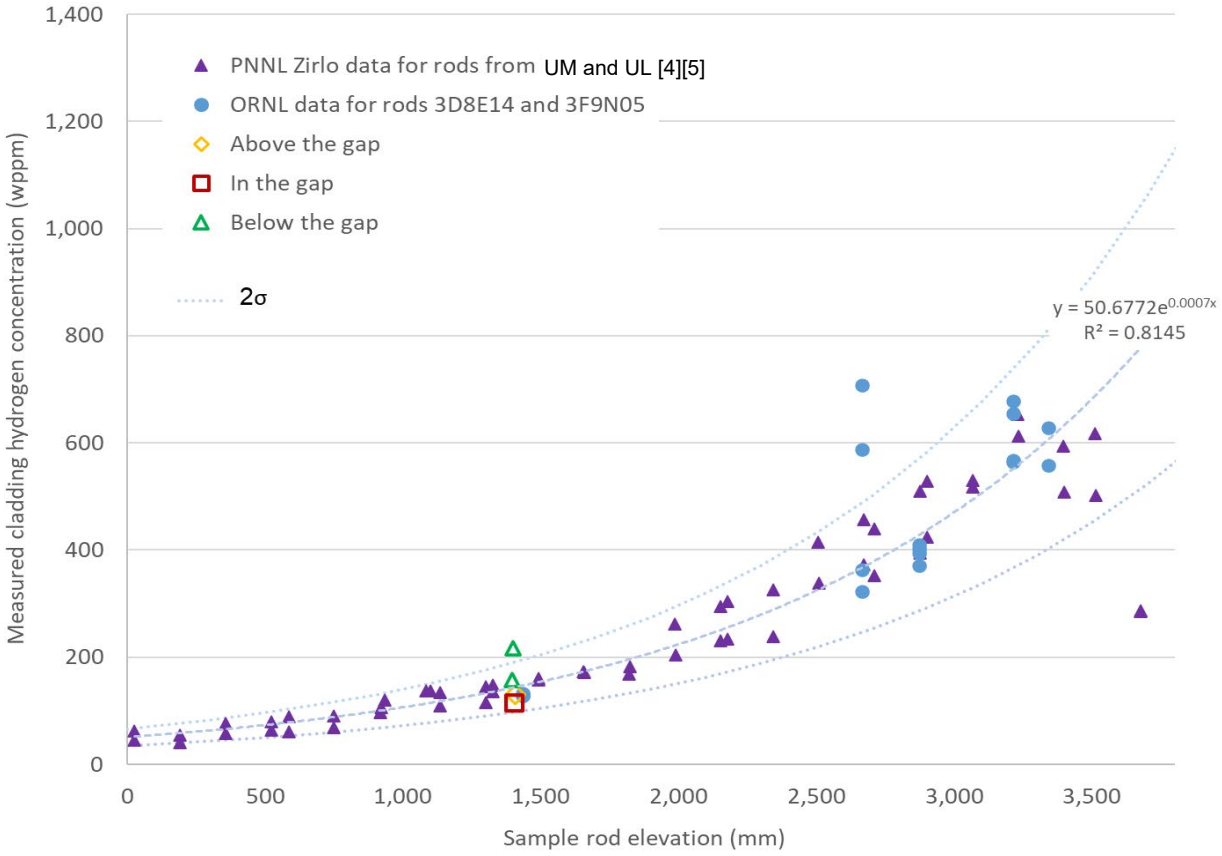

Figure 6. Measured cladding hydrogen concentration as a function of rod elevation for the samples taken above, below, and in the pellet–pellet gap compared with data from the same and other comparable ZIRLO-clad rods.

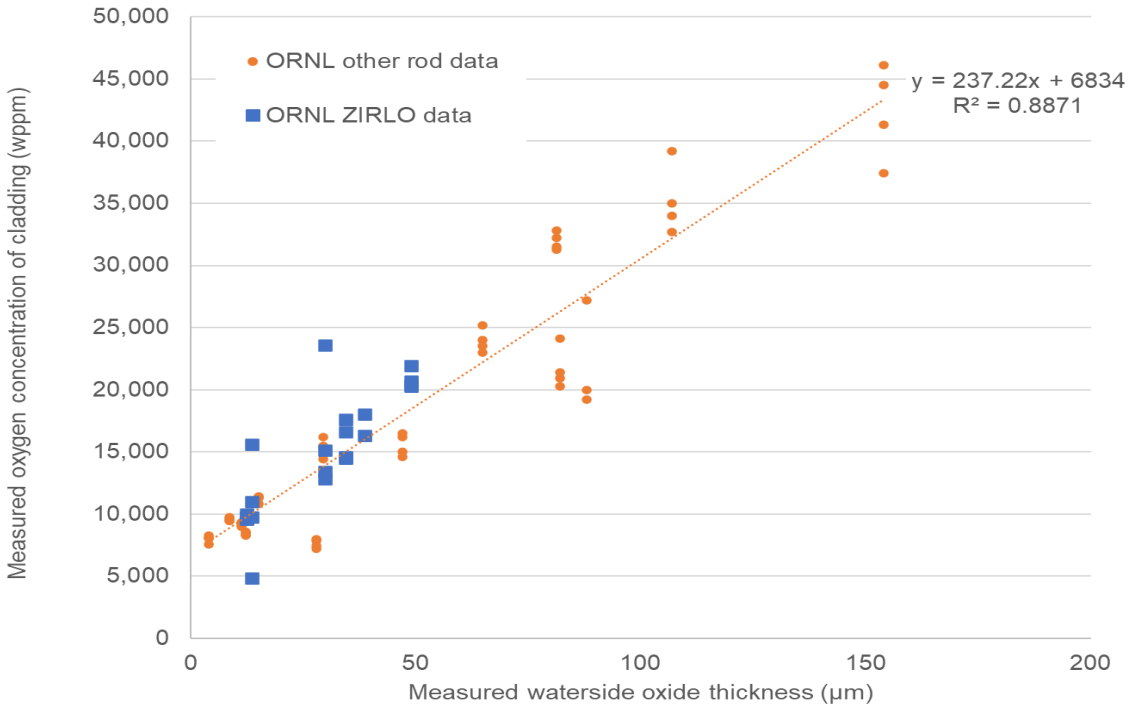

Figure 7. Measured waterside oxide thickness vs. measured cladding oxygen concentration.

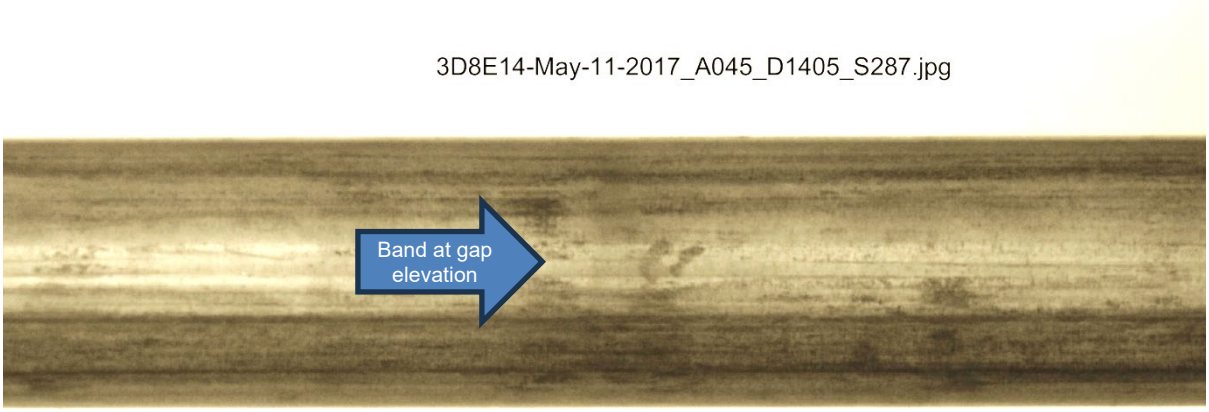

Figure 8. Waterside surface image of 3D8E14 at the pellet–pellet gap elevation.

5.1 Above the pellet–pellet gap

Above the gap, the oxygen and hydrogen concentrations are as expected. The measured hydrogen is 131 wppm and is slightly lower than expected for the elevation but well within two standard deviations for hydrogen concentration and oxygen concentration.

5.2 In the pellet–pellet gap

An examination of the data from the pellet–pellet gap indicates that the cladding has a hydrogen concentration of 115 wppm, which is about double the amount expected given its measured oxygen content of only 4850 wppm (see Figure 5). The oxygen and hydrogen values remain much lower than typical for the rod elevation if there were not a gap. These findings indicate that additional hydrogen that has diffused to the pellet–pellet gap.

5.3 Just below the pellet–pellet gap

Based on the trend with rod elevation, the sample just below the pellet–pellet gap has a measured hydrogen concentration that is above two standard deviations for hydrogen concentration at the 1402 mm elevation. Also, the oxygen measured at the 1402 mm elevation is higher than expected given the measured hydrogen concentration (Figure 4). These two facts together indicate that relatively more waterside oxidation occurred just below the gap and that some of the hydrogen from this location diffused to the pellet–pellet gap location. The sample that was farther from the gap (1408 mm) had the expected oxygen and hydrogen contents, given the waterside oxide thickness and the elevation of the sample on the rod.

6 Conclusions and future work

The results of this study indicate that hydrogen diffused to the pellet–pellet gap, but only from the elevation just below the gap. The magnitude of the diffusion was not enough to increase the gap cladding hydrogen content to the concentration of the cladding above and below it, and the hydrogen concentration remained lower than typical for that rod elevation. The reason for the increased hydrogen and oxygen concentration just below the gap is unknown.

The rod configuration should be modeled to investigate the measured result.

7 Acknowledgements

This material is based upon work supported by the US Department of Energy, Office of Nuclear Energy, under the Spent Fuel and Waste Disposition's Spent Fuel and Waste Science and Technology Campaign as part of the High Burnup Spent Fuel Data Project.

8 References

1. Montgomery, R., Bevard, B. B., Harp, J., Jordan, T., Curlin, S., Dixon, T., Pan, G., Mitchell, D., Brookmire, T., and Clemens, C. “Characterization of fuel and cladding in and near the pellet–pellet gap of a high-burnup pressurized water reactor fuel rod.” *Proceedings of the 2021 Water Reactor Fuel Performance Meeting*, American Nuclear Society, United States.
2. Courty, O., Motta, A. T., and Hales, J. D. “Modeling and simulation of hydrogen behavior in Zircaloy-4 fuel cladding.” *Journal of Nuclear Materials* 452 (2014) 311–320.
3. Weick, S., Grosse, M., Steinbrück, M., Stuckert, J., Herm, M., Seifert, H. J., Boldt, F. “The SPIZWURZ project with new approaches for experiments and modelling related to long-term dry storage.” *Proceedings of TopFuel 2022 Light Water Reactor Fuel Performance Conference*.
4. Shimskey, R. W., et al. *PNNL FY 2021 Sibling Pin Testing Results*. M2SF-21PN010201057 M2SF-22PN010201062 PNNL-32783, Pacific Northwest National Laboratory (2022).
5. Shimskey, R. W., et al. *PNNL FY 2022 Sibling Pin Testing Results*. M2SF-23PN010201041 PNNL-33781, Pacific Northwest National Laboratory (2023).